A Two-Stage Control Scheme of Single-Link Flexible Manipulators

Andres San-Millan[1], Vicente Feliu[1] and Alfonso Garcia[2]

***Abstract*— A new control scheme composed of two independent stages utilised to achieve precise positioning of single-link flexible manipulators is presented herein. Traditional techniques for the control of single-link flexible manipulators utilise only one actuator and two types of sensor measurement (e.g the angular position of the motor and acceleration or strain measurements) to move the manipulator and in order to damp the residual vibrations produced in the displacement of the manipulator. However, in the proposed control scheme another additionally pair actuator-sensor is utilised to improve the speed and precision of the controlled system. On the one hand a motor and the readings of a rotary encoder are utilised in a first stage to displace the manipulator, using the strain measurements in order to damp the high amplitude and low frequency residual vibrations. On the other hand piezoelectric actuators are utilised in conjunction with displacement measures of the tip of the manipulator in order to damp the low amplitude and high frequency residual vibrations which deteriorate the accuracy of the positioning achieved by the traditional control techniques. Simulation and experimental results are carried out to illustrate these improvements.**

***Index Terms*— Flexible manipulator, Flexible link, Smart materials, Piezoelectric, Robot control.**

I. INTRODUCTION

In contrast with the traditional rigid manipulators "flexible robots" or "flexible manipulators" exhibit many advantages such as reduced weight. This reduction in the overall weight of the robot allows the utilisation of smaller actuators (which also contributes to the reduction in weight), and the utilisation of smaller amounts of energy to drive the manipulator. These advantages make them ideal for applications in the aerospace industry. Additionally, due to their reduced inertia and flexibility (which allows them to easily transform kinetic energy into potential energy), flexible manipulators are safer to operate near to humans. However the flexibility of their links determines the apparition of residual vibrations, which make accurate positioning or trajectory tracking a challenging task, motivating a huge research in this topic [1].

Many control techniques have been applied to flexible robots in order to remove the apparition of residual vibration and increase the accuracy of the tip-positioning. Some representative examples are adaptive control [2], [3], [4], and robust control [5], [6], [7]. Both approaches share a common characteristic: they utilise only the motor in order to move the manipulator and remove the residual vibrations. The utilisation of only one type of actuation determines the need of complex design methodologies, which additionally can show unstability issues due to the spillover effects.

On the other hand, the active vibration control of the so-called "smart structures" has been intensively investigated in the recent years. Due to their piezoelectric properties and, potential benefits in vibration suppression of lightweight flexible structures, materials such as lead zirconate titanate (PZT) are employed as actuators in these structures. Bonding piezoelectric patches in a structure can effectively remove vibration produced by external perturbations [8], [9].

Using both strategies can improve the performance of flexible manipulators by combining the advantages of each approach and avoiding their drawbacks, i.e. the piezoelectric actuators (PEAs) utilised in the smart structures provide a high bandwidth but small stroke and, the motor utilised to move the flexible robot can provide a long stroke but small bandwidth. Combining both actuators allows to take advantage of the stroke of the motor and the bandwidth of the PEA.

This hybrid approach has already been studied in previous works, where a proportional term is utilised to control the PEA, and PD schemes [10], [11], [12] or Sliding controllers [13] are utilised to control the angular position of the motor of the robot. However these works present the following drawbacks: 1) The control of the motor is utilised only to rotate the manipulator without damping the vibrations that might arise. 2) The PEA is actuated simultaneously to the rotation of the robot, which may saturate the PEA when the motor produces fast movements. 3)The utilisation of a PD controller does not guarantee a zero steady error. 4) The stability of the control scheme is not guaranteed under big changes of payload.

In the present work, the scheme used to control the angular position of the motor is utilised not only to achieve a precise positioning without zero steady error, but also to damp the vibrations of the first resonant mode of the flexible link.

The proposed control scheme is based on [14], [15], where it is presented a passivity-based control scheme consisting of two nested loops, which are designed independently, by decoupling joint and link dynamics with a linear strain feedback. In these works the residual vibration, which appears after the movement of the robot, is damped, resulting in control schemes robust against the Coulomb friction of the motor, changes in the parameters of the system, and to spillover effects. It is important to note that this first stage of control allows to achieve a zero steady-state error.

*This paper was sponsored by the Spanish FPU12/00984 Program (Ministerio de Educacion, Cultura y Deporte). It was also sponsored by the Spanish Government Research Program with the Project DPI2012-37062-CO2-01 (Ministerio de Economia y Competitividad) and by the European Social Fund.

[1]A. San-Millan and V. Feliu are with the Universidad de Castilla-La Mancha, Ciudad Real 13071, Spain (e-mail: andres.sanmillan@uclm.es; vicente.feliu@uclm.es)

[2]A. Garcia is with the Universidad de Malaga, Malaga 29071, Spain (e-mail: alfonso.garcia@isa.uma.es)

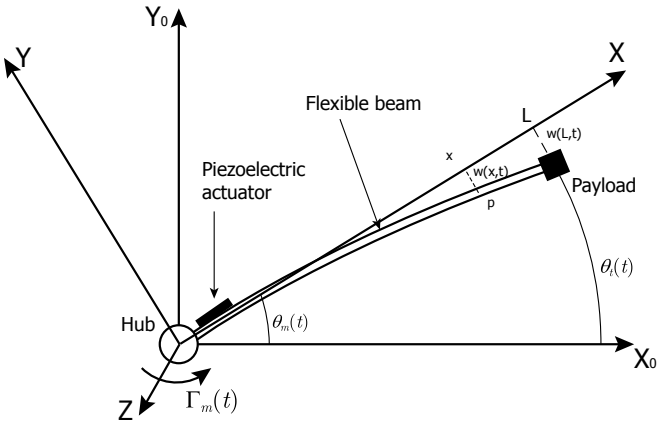

Fig. 1. Robotic system scheme

Additionally, the control strategy adopted in [15] is improved by adding a second control stage consisting on the PEA control using linear velocity feedback, named L-type control. The linear velocity feedback is measured by means of a laser vibrometer.

The addition of the extra control stage and the extra actuator and sensor allows to improve the accuracy of the controlled system by increasing the damping of the high frequency residual vibrations, which cannot be removed by means of the DC motor.

II. DYNAMIC MODELLING

The schematic representation of the system to be controlled is shown in Fig. 1. The system can be divided in two subsystems: a) a motor and a reduction gearbox of 1:n at the base with rotor and hub inertia J_0, viscous friction coefficient ν, and Coulomb friction torque Γ_f; b) a flexible beam with uniform mass density per unit length ρ, uniform bending stiffness EI, length L, and a payload of mass m and negligible rotational inertia.

Additionally the torque applied by the motor is $\Gamma_m(t)$, $w(x,t)$ in the elastic displacement measured from the rigid beam at the point x in the time instant t, $\theta_m(t)$ is the motor angle, and $\theta_t(t)$ is the tip angle. $M_p(x,t)$ is the induced piezoelectric moment (which is K_p times the voltage applied to the PEA $V_p(t)$, and it is also proportional to the location x of the PEA along the link).

In order to deduce the equations of the dynamic model, the pseudo-clamped configuration [16] is utilized. Therefore, the non-inertial frame (X,Y) rotates with the motor and the overall structure rotates in an inertial frame (X_0,Y_0). It is important to note that the movement is constrained to the horizontal plane and the gravity effects are negligible.

Both subsystems (the motor and the flexible link) present a strong interaction between them, which can be seen in the equation of the momentum balance at the output side of the reduction gearbox:

$$\Gamma_m(t) = nK_mV_m(t) = J_0\ddot{\theta}_m(t)+\nu\dot{\theta}_m(t)+\Gamma_f(t)+\Gamma_{coup}(t) \quad (1)$$

where V_m is a voltage that controls the motor; K_m is a constant that relates the motor torque Γ_m and the control voltage V_m; and Γ_{coup} is the coupling torque produced by the link and the payload, this coupling torque can be obtained using the following expression:

$$\Gamma_{coup}(t) = -EIw^{''}(0,t), \quad (2)$$

where $w^{''}(0,t)$ is proportional to the strain measured at the base of the link and, where $(')$ represents the derivative with respect the variable x.

By considering the link as an Euler-Bernoulli beam, taking the assumption of small deflections, and taking into account the presence of the piezoelectric actuators placed at the base of the link, the linearized equations of motion can be derived from energy equations and by using the Hamilton principle as follows:

$$\rho\left(x\ddot{\theta}_m + \ddot{w}\right) + EI\frac{\partial^4 w}{\partial x^4} = \frac{\partial^2 M_p}{\partial x^2} \quad (3)$$

where $(\dot{})$ is used for time derivatives.

The geometrical and natural border conditions are:

$$w(0,t) = 0 \quad (4)$$

$$\frac{\partial w}{\partial x}(0,t) = 0 \quad (5)$$

$$EI\frac{\partial^2 w}{\partial x^2}(L,t) = M_p(x,t) \quad (6)$$

$$EI\frac{\partial^3 w}{\partial x^3}(L,t) = m\left(L\ddot{\theta}_m(t) + \ddot{w}(L,t)\right) + \frac{\partial M_p w}{\partial x}(L,t) \quad (7)$$

By solving this boundary value problem the dynamical behaviour of the whole system can be modelled. Additionally, considering again small deflections, it can be defined the tip angle $\theta_t(t)$ as:

$$\theta_t(t) = \theta_m(t) + \frac{w(L,t)}{L}, \quad (8)$$

and the speed of the tip can be defined as the time derivative of $\theta_t(t)$

It is important to note that, in the experimental platform utilised in this work, θ_m and $w^{''}(0,t)$ can be measured directly, but the speed of the tip is measured by means of a laser vibrometer which only provides measurements when the angular position of the motor is stopped at an angle so that the link is facing the laser perpendicularly. The speed measurements of the laser vibrometer can therefore be defined as follows:

$$v_t(t) = \dot{w}(L,t). \quad (9)$$

The whole model of the system can be particularized to the open-loop diagram of Fig. 2, where it can be seen the strong coupling between the dynamics of the motor and the flexible beam.

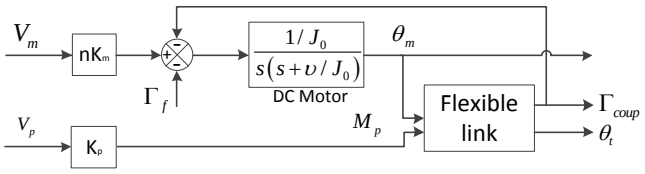

Fig. 2. Dynamics of a single-link flexible manipulator

As it can be seen in Fig. 2, the system can be classified as a Multiple-input Multiple-output (MIMO) system, where the inputs to the system are V_m and V_p (Γ_f is considered a perturbation to the system), and the outputs of the system are θ_m, Γ_{coup}, and θ_t. However, in order to reduce the complexity of the system, the MIMO system is divided in two consecutive Single-input Single-output (SISO) systems by means of the following assumptions: initially, only the motor would be utilised to move the system, (which implies $V_p = 0$) and, after certain time, the motor is braked and only the PEA would be utilised to control the system , (which implies $\dot{\theta}_m = 0$ and, therefore $\dot{\theta}_t = v_t$). Under these assumptions, the system can be seen as two independent SISO systems which are switched at certain instant.

This approach is utilised not only to reduce the complexity of the system to be controlled, but also because of the characteristics of the actuators of the system i.e. small bandwidth and high stroke for the motor, and high bandwidth and small stroke for the PEA. Since the residual vibrations induced by the movement of the robot are composed of an infinite number of harmonics, the low frequency and high amplitude harmonics can be removed only by means of the motor, whereas the high frequency, low amplitude harmonics can be removed by the PEA.

When the two SISO systems are analysed independently, it can be seen that the transfer function which relates $\Gamma_{coup}(t)$ and $\theta_m(t)$ can be expressed as:

$$\frac{\Gamma_{coup}(s)}{\theta_m(s)} = G_1(s) = \sum_{i=1}^{N} \frac{\sigma_i \omega_i^2}{s^2 + 2\zeta_i \omega_i s + \omega_i^2}, \qquad (10)$$

where $N \to \infty$, σ_i corresponds to the gain of each mode of vibration, ζ_i is the damping ratio of each mode, and ω_i is the natural frequency of vibration of each mode. It can be seen from (10) that the pair sensor-actuator determined a collocated system.

On the other hand, when the the transfer function which relates $V_p(t)$ and $v_t(t)$ is analysed, the following expression is obtained:

$$\frac{v_t(s)}{V_p(s)} = G_2(s) = \sum_{i=1}^{N} \frac{(-1)^i \sigma_i \omega_i^2 s}{s^2 + 2\zeta_i \omega_i s + \omega_i^2}, \qquad (11)$$

In this case, it can be seen from (11) that the pair sensor-actuator determines a non-collocated system, which is more complicated to control. Note that since $\dot{\theta}_t = v_t$, controlling the speed of the tip of the flexible link so that $v_t = 0$ would lead to a precise positioning of the tip of the link, being $\theta_t = \theta_m$.

III. Control design methodology

As it can be seen from (1), the relationship between the angular position of the motor θ_m and the voltage applied to the motor V_m is strongly influenced by the coupling torque generated by the interaction between the motor and the flexible link. In order to make the design of the control scheme of the motor independent of the link dynamics, a decoupling term is added as follows:

$$V_m(t) = V_m^c(t) + \Gamma_{coup}(t)/(nK_m), \qquad (12)$$

$V_m^c(t)$ being a fictitious voltage control signal. If $V_m(t)$ is substituted in (1), the following equation is obtained:

$$nK_m V_m^c(t) = J_0 \ddot{\theta}_m(t) + \nu \dot{\theta}_m(t) + \Gamma_f(t) \qquad (13)$$

which corresponds to a motor without load. By using this decoupling term, the equivalent dynamics of the actuator is not influenced by the link dynamics, resulting in the following transfer function (when the Coulomb friction is neglected):

$$\frac{\theta_m(s)}{V_m^c(s)} = \frac{1/J_0}{s(s + \nu/J_0)} \qquad (14)$$

In the remaining of this section it is detailed the control design methodology proposed to control both the DC motor of the robot and the PEA situated at the base of the flexible link. Combining both actuators leads to an improvement in the precise positioning of the manipulator, compared with the utilisation of the DC motor only. In this work, the DC motor is utilised to rotate the manipulator and, simultaneously, compensate the high amplitudes of the low frequency vibrations produced during the movement. On the other hand, the utilisation of a PEA allows to compensate the remaining residual high frequency vibrations which cannot be compensated with the motor due to its small bandwidth. It is important to note that since the PEA presents a small stroke, it can only damp small amplitude vibrations.

In order to combine both actuators, two different control schemes are designed (one for each utilised actuator), and applied in two sequential steps. The sequential actuation of each actuator allows to simplify the design of the controller utilised in each stage. It is important to note that the variable fed back in order to damp the vibrations with the motor is Γ_{coup} (which is related to the strain measurement at the base of the link), which is strongly influenced by the induced piezoelectric moment $M_p(x,t)$ and, therefore, a simultaneous operation of both actuators would lead to a distortion in the strain measurement.

The overall control process is therefore divided in two stages: the first one rotates the flexible link to the desired angular position, and damps the residual vibrations with low frequency and high amplitude (typically the first harmonic); in the second stage, when the desired angular position has been reached and the high amplitude vibrations have been

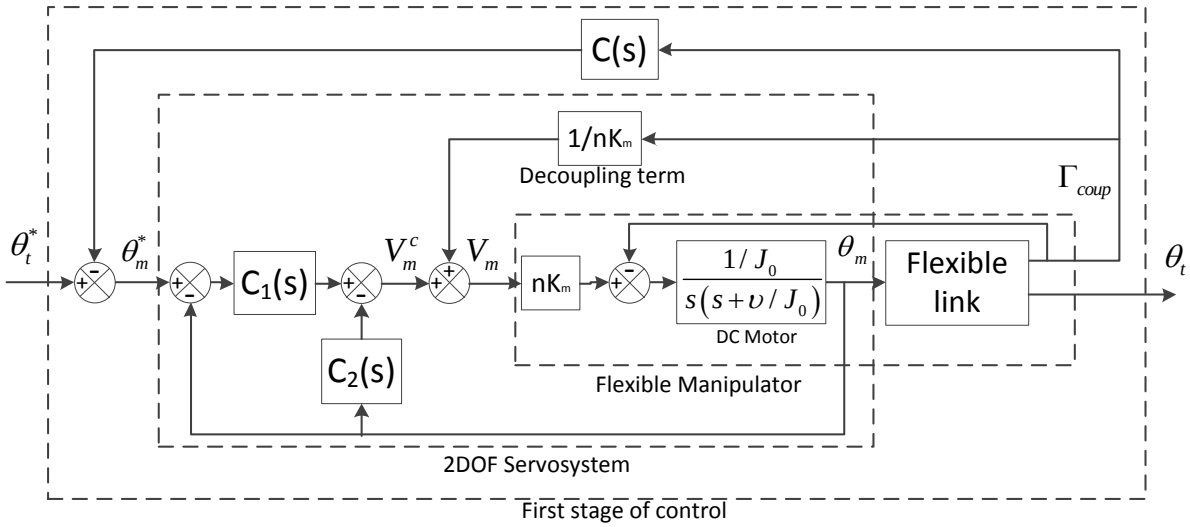

Fig. 3. First control stage

removed, the first controller is switched off, and the second controller is activated. In this second controller, the evolution of $v_t(t)$ is utilised to drive the PEA (bonded to the base of the flexible link) in order to remove the high frequency residual vibrations, and to reduce the time the system takes to reach a steady position without any vibration.

A. First control stage

In order to design a suitable controller for the first stage of control it was utilised the controller proposed in [15]. This controller was chosen because it is robust against large changes in the payload and to spillover effects, and because it has got a zero steady-state error (which is a necessary condition to guarantee the measurements of $v_t(t)$ in the second control stage). It is important to note that since this control scheme relies on the passivity property between $\int \Gamma_{coup}$ and θ_m demonstrated in [17], the stability of the control scheme is guaranteed even in the presence of changes in the payload of the robot.

The goal of this first controller is to achieve a precise positioning of the tip of the flexible link. It is important to note that, as stated in Section II, the angle of the tip of the link is not the same as the angle of the motor because of the deflection of the link.

According to (8), if there is no deflection in the link (which means that the link behaves like a rigid body or that the vibrations of the link have been removed), controlling the angular position of the motor would lead to a precise positioning of the tip of the manipulator.

The control design methodology utilised in this first stage consists of three sequential steps: first, the decoupling between the link and motor dynamics is achieved by adding a decoupling term (12) by using a direct feedback of the coupling torque measured with a straing gauge placed at the base of the link; then a two-degree of freedom (2DOF) servocontroller is designed to control the angular position of the motor and remove the effects of any non-linearity present in the motor caused by the friction; and finally an outer control loop is designed in order to damp the vibrations of the tip of the link by taking as feedback the coupling torque. The complete block diagram of the first stage of control can be seen in Fig. 3

As can be seen in Fig. 3, the 2DOF controller is composed by the blocks $C_1(s)$ and $C_2(s)$ which present the following forms:

$$\begin{aligned} C_1(s) &= \frac{a_2 s^2 + a_1 s + a_0}{s^2 + gs} \\ C_2(s) &= \frac{b_1 s + b_0}{s + g}. \end{aligned} \tag{15}$$

The coefficients of $C_1(s)$ and $C_2(s)$ are obtained by following the design criteria detailed in [15]. The design is made bearing in mind that the goal is to obtain a closed-loop response for θ_m as fast as possible and a zero tracking error in the steady state. In order to achieve such response, the design criteria minimises the following functional:

$$T_f = \int_0^\infty (\theta_m^*(t) - \theta_m(t))^2 t dt, \tag{16}$$

where $\theta_m^*(t)$ is the reference of angular position of the motor.

Once a controller has been designed for the motor such that it can follow the reference of the angular position θ_m^*, another control loop is designed in order to damp the residual vibrations which appear after the link is rotated. This controller $C(s)$ is designed so that the passivity condition existing between the integral of Γ_{coup} and θ_m is guaranteed. The transfer function of this block is:

$$C(s) = \frac{K_c(s + \lambda)}{s} \tag{17}$$

The parameters of (17) are chosen such that the closed-loop poles of the system which determine the behaviour of the first harmonic are placed as far as possible form the

imaginary axis (increasing the damping for the first mode of vibration).

It can be seen that by using this controller, only the first harmonic is substantially damped (since only the location of the poles of the first harmonic is considered in the design criteria). The harmonics with a frequency higher than the first one would therefore present an undamped behaviour.

B. Piezoelectric control

In order to increase the damping of the remaining harmonics of the system, the second control stage takes as measurement the linear speed of the tip of the link and it utilises the PEA bonded to the base of the link to damp the vibrations.

It is important to notice that, since the actuator and the sensor are not placed at the same position, the system is non-collocated, which makes extremely difficult to achieve the stability [18] due to the non minimum phase behaviour of the system. It can be seen from (11) that the nonminimum phase feature does not significantly affect the magnitudes, but the phase is substantially influenced (each mode of vibration is displaced 180° from the previous one). If a classical controller (P,PD, or PID) is utilised to close the control loop, there will be always an infinite number of poles that will lie in the positive half-plane because of the nonminimum phase zeros of the system.

Traditionally, the control scheme utilised to control these systems is based on a lead compensator plus a filter (usually a notch filter) tuned in such a way that only the first harmonic of the system is controlled [19]. The principle behind these kind of controllers is that, in one hand, the lead compensator allows to compensate the phase shift of the target harmonic and, on the other hand, the filter restricts the control action only to the desired harmonic, leaving the remaining harmonics unaltered.

In this article, the combination of several band-pass filters in parallel is utilised in order to control each mode of vibration of the flexible link independently. Furthermore, since the odd harmonics have a phase shift of 180° from the even harmonics, each bandpass filter has got associated a lead compensator in order to remove the phase shift (since the phase shift is 180°, the lead compensator consists of a change of sign).

The proposed control scheme can be seen in Fig. 4 where each band-pass filter F_i has got the transfer function of an unitary gain Butterworth band-pass filter centered in the natural frequencies of the flexible link as follows:

$$F_i(s) = -1^i \frac{B_I s}{s^2 + B_i s \omega_i^2}. \tag{18}$$

Here the bandwidth of each filter B_i is chosen by using the following relationship:

$$B_i = \omega_i \sqrt{(2)}/2 \tag{19}$$

It can be seen from Fig. 4 that the utilised controller is a typical proportional controller, and that the effect of the band-pass filters is on the one hand to limit the control signal produced by the proportional controller to a limited band of frequencies, and on the other hand to compensate the phase shift of the even harmonics (the changes of sign) in (11). It is important to note that the application of band-pass filters allows not only to separate the control signal of each harmonic, but also to guarantee the robustness of the system against the effects of the spillover, since at high frequencies (usually the unmodelled ones) the control action is equal to zero.

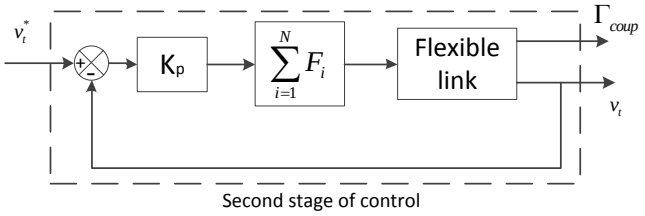

Fig. 4. Second control stage

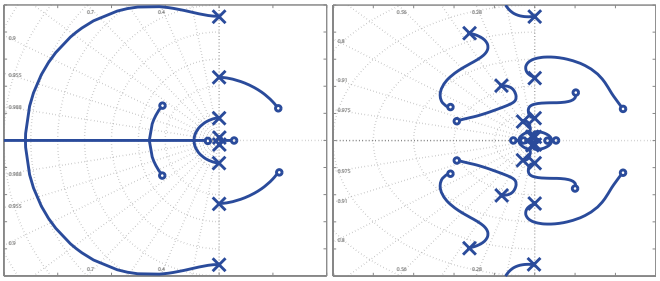

Fig. 5. Root locus of a non-collocated system. (a) without band-pass filters in the control action, (b) with band-pass filters in the control action

The value of the proportional controller is chosen so that the closed-loop poles of the identified harmonics are situated as far as possible from the imaginary axis by using the root locus of the closed-loop system with the previously designed band-pass filters. A comparison between the root locus of the closed-loop system with and without the bandpass filters can be seen in Fig. 5

It can be seen from Fig. 5 that, if there is no band-pass filter applied to the system, the closed-loop system is unstable for any value of the gain K_p. However, when the filters are applied, the shape of the root locus is more complex, but there is a range of acceptable values of K_p which produce a stable behaviour of the system, and where the location of the closed-loop poles is further away from the imaginary axis than in the open loop. By using this root locus, the value of K_p can be adjusted.

C. Combined control scheme

In this subsection the algorithm utilised to switch between the two aforementioned control algorithms is detailed. The two control stages together with the switching blocks can be seen in Fig. 6

As it can be seen in Fig. 6, the overall controller works in the following way: when there is a change in the reference

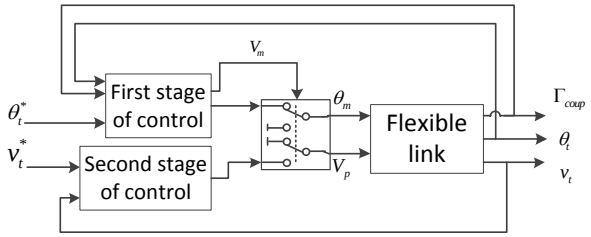

Fig. 6. Complete control scheme

θ_t^* (because the manipulator is going to move to a new angular position), the switch of the first control stage is turned on so that the servosystem can change the angular position of the motor and damp the first mode of vibration. When the desired angular position is reached and the first vibration mode is damped, the voltage applied to the motor becomes approximately zero. In order to switch between control stages, the applied voltage to the motor has to meet the following condition:

$$\frac{\sum_{i-N}^{i} |V_m(i)|}{N} \leq \mu \tag{20}$$

where N represents the number of considered samples to compute the mean absolute value of V_m, and μ represents a threshold value (close to zero). The values of N and μ are chosen based on the experience of the designer, in order to guarantee a safe commutation.

When the commutation of both controllers is triggered, on the one hand, the switch of the first control stage is turned off so that the voltage applied to the motor is held at a zero value; and on the other hand, the switch of the second control stage is turned on, so that the PEA acts over the flexible link, damping the remaining high frequency vibrations. Finally, when all the vibrations have been removed, the system is reset to the original state.

IV. EXPERIMENTAL RESULTS AND SIMULATIONS

The identification of the motor dynamics was firstly carried out. This dynamics is as follows:

$$\frac{\theta_m(s)}{V_m(s)} = \frac{39.26}{s(s+4.24)} \tag{21}$$

Based on this model, the servo controller of the first control stage was computed. The transfer functions designed for each block were the following:

$$C_1(s) = \frac{2.06s^2 + 2801.7s + 950000}{s^2 + 1371.8s} \tag{22}$$

$$C_2(s) = \frac{12218s + 210000}{s + 1371.8} \tag{23}$$

Subsequently, the transfer function (10) was identified from the experimental platform:

$$\begin{aligned}\frac{\Gamma_{coup}}{\theta_m} =& \frac{5s^2}{s^2 + 0.075s + 43.42} + \frac{3.5s^2}{s^2 + 0.131s + 1720.2} \\ &+ \frac{3s^2}{s^2 + 0.417s + 13439} + \frac{3s^2}{s^2 + 0.821s + 52020}\end{aligned} \tag{24}$$

Once the dynamics of the flexible link is known and the servosystem has been designed, the outer control loop of the first control stage can be designed. After the tuning process has been completed, the values obtained of the controller's parameters were the following:

$$C(s) = \frac{0.84(s + 4.76)}{s} \tag{25}$$

Once the first control stage has been designed, the parameters of the switching condition (20) were tuned. It was found that the optimal parameters were $N = 10$ samples and $\mu = 0.01$.

Next, the transfer function corresponding to (11) was identified from the experimental platform:

$$\begin{aligned}\frac{v_t}{V_p} =& \frac{-0.01475s}{s^2 + 0.07512s + 43.42} + \frac{0.07578s}{s^2 + 0.1309s + 1725} \\ &+ \frac{-0.1802s}{s^2 + 0.4189s + 13540} + \frac{0.2458s}{s^2 + 0.824s + 52390}\end{aligned} \tag{26}$$

Finally the second stage of the controller is designed by using (18) and (19), and by using the root locus of the closed system to adjust the parameter K_p, obtaining the following equations:

$$\begin{aligned}F_1 = \frac{-4.659s}{s^2 + 4.659s + 37.99}, F_2 = \frac{29.37s}{s^2 + 29.37s + 1510}, \\ F_3 = \frac{-82.28s}{s^2 + 82.28s + 11850}, F_4 = \frac{161.9s}{s^2 + 161.9s + 45840}, \\ K_p = 153\end{aligned} \tag{27}$$

The application of the controller (27) over the transfer function of the flexible link defined by (26) places the closed-loop poles of the system further away from the imaginary axis than the open loop, increasing the damping of all the considered modes of vibration as it can be seen in Fig. 7

The results obtained applying a step input of amplitude equal to 0.5 radians to the controlled system are shown in Figs. 8 and 9. It can be seen that the steady state error of the system is null and the residual vibration is approximately zero after 3s.

Since the error in the tracking of the motor angular position reference is equal to zero after 3s, and the vibrations produced by the first harmonic have been highly damped, the activation of the second control stage is produced. Fig. 10 shows the evolution of the speed of the tip of the flexible link when the second control stage is active and when is inactive. It can be seen that the presence of the second control stage increases the damping of the high frequency residual vibrations.

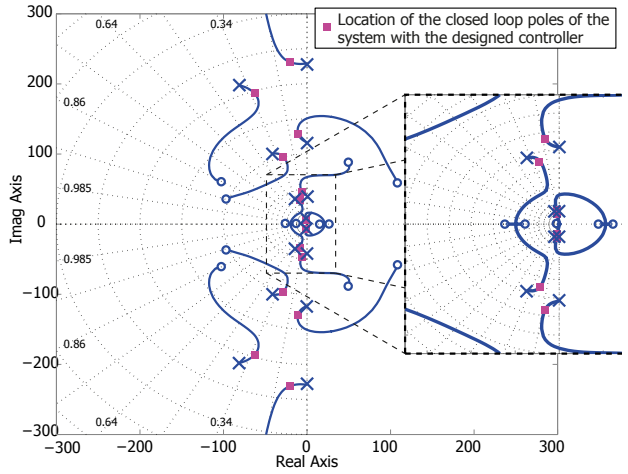

Fig. 7. Placement of the closed-loop poles with the application of the piezoelectric control

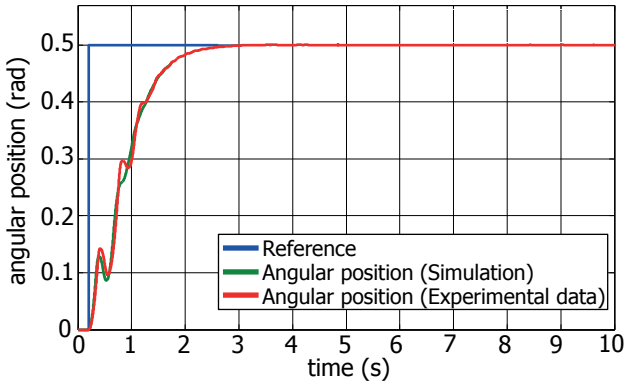

Fig. 8. Evolution of the angular position of the motor

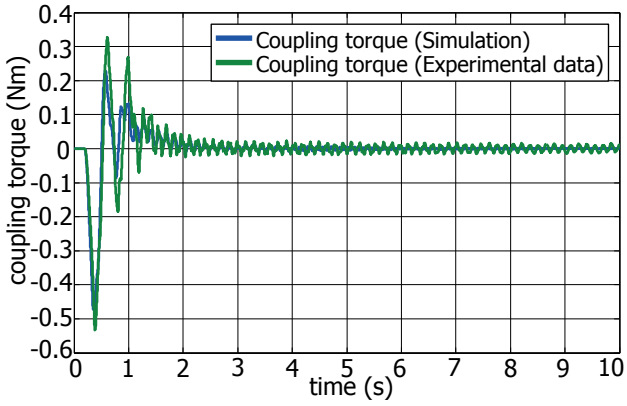

Fig. 9. Evolution of the coupling torque

V. CONCLUSIONS

This work has proposed an extension of a previous passivity based control scheme for single link flexible manipulators, in order to nearly completely damp small high frequency residual vibrations. This extension is based on the addition of a new pair sensor-actuator and on the addition of a new control stage to drive the additional actuator. Furthermore, it has been developed a criterion to determine the exact instant at which each actuator has to be activated. The resulting control scheme has been simulated and implemented in a laboratory setup, showing its effectiveness in removing the steady state error position and the residual vibrations of high and low frequencies, reducing in this way the time needed by the system to reach its steady state.

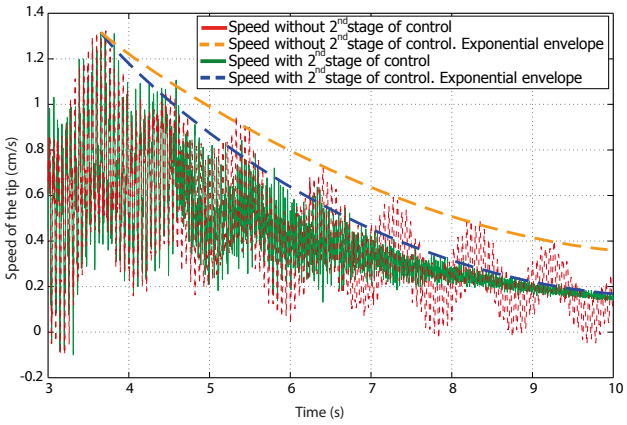

Fig. 10. Evolution of the speed of the tip of the link

REFERENCES

[1] V. Feliu. Robots flexibles: Hacia una generacin de robots con nuevas prestaciones. *Revista Iberoamericana de Automtica e Informtica Industrial*.

[2] T.C. Yang, J.C.S. Yang, and P. Kudva. Load-adaptive control of a single-link f lexible manipulator. *Systems, Man and Cybernetics, IEEE Transactions on*, 22(1):85 –91, jan/feb 1992.

[3] J.J. Feliu, V. Feliu, and C. Cerrada. Load adaptive control of single-link flexible arms based on a new modeling technique. *Robotics and Automation, IEEE Transactions on*, 15(5):793 –804, oct. 1999.

[4] A.G. Dharne and S. Jayasuriya. Robust adaptive control of residual vibration in point-to-point motion of flexible bodies. *Journal of Vibration and Control*, 13(7):951–968, 2007.

[5] Y.P. Chen and H.T. Hsu. Regulation and vibration control of an fem-based single- link flexible arm using sliding-mode theory. *Journal of Vibration and Control*, 7(5):741–752, 2001.

[6] M. Amiri, M.B. Menhaj, and M.J. Yazdanpanh. A neural-network-based controller for a single-link flexible manipulator: Comparison of ffnn and drnn controllers. In *Neural Networks, 2008. IJCNN 2008. (IEEE World Congress on Computational Intelligence). IEEE International Joint Conference on*, pages 1686 –1691, june 2008.

[7] V.G. Moudgal, W.A. Kwong, K.M. Passino, and S. Yurkovich. Fuzzy learning control for a flexible-link robot. *Fuzzy Systems, IEEE Transactions on*, 3(2):199 –210, may 1995.

[8] Riessom Weldegiorgis, Prasad Krishna, and K.V. Gangadharan. Vibration control of smart cantilever beam using strain rate feedback. *Procedia Materials Science*, 5(0):113 – 122, 2014. International Conference on Advances in Manufacturing and Materials Engineering, {ICAMME} 2014.

[9] Dafang Wu, Liang Huang, Bing Pan, Yuewu Wang, and Shuang Wu. Experimental study and numerical simulation of active vibration control of a highly flexible beam using piezoelectric intelligent material. *Aerospace Science and Technology*, 37(0):10 – 19, 2014.

[10] Dong Sun and James K. Mills. Control of a rotating cantilever beam using a torque actuator and a distributed piezoelectric polymer actuator. *Applied Acoustics*, 63(8):885 – 899, 2002.

[11] Dong Sun, Jinjun Shan, Yuxin Su, Hugh H T Liu, and Chiming Lam. Hybrid control of a rotational flexible beam using enhanced pd feedback with a nonlinear differentiator and pzt actuators. *Smart Materials and Structures*, 14(1):69, 2005.

[12] Joo C.P. Reis and Jos S da Costa. Control of a single flexible-intelligent link robot. In *ACD 2009 - 7th Workshop on Advanced Control and Diagnosis Zielona Gora, Poland*, 2009.

[13] S.B. Choi and H.C. Shin. A hybrid actuator scheme for robust position control of a flexible single-link manipulator. *Journal of Robotic Systems*, 13(6):359–370, 1996.

[14] Vicente Feliu, Emiliano Pereira, and Ivn M. Daz. Passivity-based control of single-link flexible manipulators using a linear strain feedback. *Mechanism and Machine Theory*, 71(0):191 – 208, 2014.

[15] AndrsSan-Milln Rodrguez and EmilianoPereira Gonzlez. Passivity-based control improvement of single-link flexible manipulators by a two-degree-of-freedom pid motor controller. In Manuel A. Armada, Alberto Sanfeliu, and Manuel Ferre, editors, *ROBOT2013: First Iberian Robotics Conference*, volume 253 of *Advances in Intelligent Systems and Computing*, pages 117–126. Springer International Publishing, 2014.

[16] F. Bellezza, L. Lanari, and G. Ulivi. Exact modeling of the flexible slewing link. In *Robotics and Automation, 1990. Proceedings., 1990 IEEE International Conference on*, pages 734–739 vol.1, 1990.

[17] E. Pereira, I.M. Diaz, J.J.L. Cela, and V. Feliu. A new design methodology for passivity-based control of single- link flexible manipulators. In *Advanced intelligent mechatronics, 2007 IEEE/ASME international conference on*, pages 1 –6, sep. 2007.

[18] Zhi cheng Qiu, Jian da Han, Xian min Zhang, Yue chao Wang, and Zhen wei Wu. Active vibration control of a flexible beam using a non-collocated acceleration sensor and piezoelectric patch actuator. *Journal of Sound and Vibration*, 326(35):438 – 455, 2009.

[19] A. Preumont. *Vibration Control of Active Structures: An Introduction*. Solid Mechanics and Its Applications. Springer, 2011.